THE ASTROPHYSICAL JOURNAL, 479:694–701, 1997 April 20

INFRARED SPECTROSCOPY OF BLUE DWARF GALAXIES

L. VANZI[1] AND G. H. RIEKE[2]

Received 1996 July 15; accepted 1996 October 29

ABSTRACT

We present a survey of the near-infrared emission lines of eight blue dwarf galaxies. These galaxies have advantages for study of the excitation of the interstellar medium by starbursts because the effects are relatively undiluted by the quiescent stellar population, the star formation episodes usually appear to be of short duration, and the effects of metallicity can be examined. Diagnostic tools for the interpretation of [Fe II](1.64) and H_2(2.12) emission lines emitted by starburst galaxies are developed and the results are compared with a starburst model. We confirm that the [Fe II](1.64) line is mainly excited in supernova remnants, but the H_2 emission appears to arise from a variety of different excitation mechanisms. Many of the galaxies show evidence for a fluorescently excited component of H_2. The temperature of the hot stellar population is analyzed by means of the He I(1.70 μm) emission line and compared with estimates from the [O III]/Hβ ratio in the optical and from the mid-infrared fine structure lines. The agreement is reasonably good, although there appears to be a tendency for the temperature to be overestimated by use of the [O III]/Hβ ratio.

Subject headings: galaxies: ISM — galaxies: starburst — infrared: galaxies — surveys

1. INTRODUCTION

Blue dwarf galaxies (BDGs) are characterized by low-luminosity $M_V \geq -18$ and very blue visible colors. Their spectra show a stellar continuum with narrow emission lines due to intense episodes of star formation. The metal content of these objects ranges from nearly 100 times lower to nearly the same as in the solar neighborhood, while the gas content is very high with a ratio of the gas to the stellar mass that can exceed one.

BDGs are unique objects for the study of starburst (SB) evolution. The radiation emitted by the star-forming regions is much less diluted by the quiescent stellar continuum than in giant spiral galaxies. The expected dependencies of SB properties on metallicity can be tested over a broad range. In most cases, there is evidence that the recent star formation has a short duration, simplifying modeling of the evolution of the young stellar population. As a consequence, starbursts hosted by BDGs are much more diversified in their characteristics than those in spiral galaxies.

We report a study of the near-infrared emission line spectra from the interstellar media in BDGs. Our goal is to use the unique attributes of these galaxies to test current hypotheses about near-infrared SB spectra, such as the excitation mechanisms for the [Fe II] and H_2 lines. We also compare measures of the temperature of the stars exciting the gas. Our observations are described in § 2. The main results are presented and discussed in § 3. The conclusions of our work are summarized in § 4.

2. OBSERVATIONS

Long-slit H and K spectra of the galaxies NGC 1569, NGC 3077, NGC 4214, NGC 4449, He 2-10, and II Zw 40 and a K spectrum of NGC 4861 were obtained with FSPEC (Williams et al. 1993) at the 2.3 m Bok telescope of Steward Observatory. A spectrum of the galaxy NGC 5253 in the H band was measured with the same spectrometer at the MMT. All the spectra have a resolution $R \approx 800$. High-resolution spectra ($R \approx 3000$) were observed for NGC 1569, NGC 3077, NGC 4449, and He 2-10. The log of the observations is given in Table 1. Data on II Zw 40 have been described elsewhere (Vanzi et al. 1996) but will be included in our analysis.

Most of the galaxies were centered successively at different positions along the slit so that for each position we could measure a sky spectrum from the adjacent spectra. Because of its large extent, for NGC 1569 we obtained pairs of spectra wobbling the telescope on and off the galaxy so the sky spectra would not be contaminated by the source.

The data reduction followed our standard procedure (e.g., Vanzi et al. 1996). Sky spectra rescaled by a suitable multiplicative factor to allow for the background variation were subtracted from the source spectra, simultaneously removing the dark current. Telluric absorptions were removed by dividing by the spectra of G stars; the false emission lines introduced with this technique were removed by multiplying by the solar spectrum as described by Maiolino, Rieke, & Rieke (1996). For wavelength calibration, we used the airglow emission lines (Oliva & Origlia 1992). From each two-dimensional image a one-dimensional spectrum was extracted with an aperture selected to optimize the S/N ratio. Where more than one bright object was detected along the slit (NGC 1569 and NGC 4214), the aperture was centered on the source showing the brightest emission lines. The apertures used for each galaxy are given in Table 1.

Images in H and K obtained at the Bok telescope with a NICMOS3 camera were used for flux calibration of the spectra. The sources were imaged at different positions on the array, and a sky frame was obtained as the median of the whole set of observations. The images were flux-calibrated using the IR photometric standards of Elias et al. (1982). The images of NGC 3077 and He 2-10 obtained on a nonphotometric night were calibrated using the observations of Aaronson (1977) and Glass & Moorwood (1985), respectively. Photometry with artificial apertures identical to those used to extract the one-dimensional spectra was used to calibrate the spectra, as summarized in Table 2. The H spectrum of NGC 5253 was calibrated using the K spec-

[1] Dipartimento di Astronomia e Scienza Dello Spazio, Universitá di Firenze, Largo E. Fermi 5, 50125, Firenze, Italy; vanzi@arcetri.astro.it.

[2] Steward Observatory, University of Arizona, Tucson, AZ 85721; grieke@as.arizona.edu.

TABLE 1

LOG OF OBSERVATIONS

Object	Band	Resolution	P.A.	t_{int} (minutes)	Aperture (arcsec)
He2-10	H	800	270	32	2.4 × 15.6
He2-10	K	800	270	32	2.4 × 15.6
He2-10	1.64	3000	270	40	2.4 × 15.6
He2-10	1.70	3000	270	40	2.4 × 15.6
He2-10	2.09	3000	270	128	2.4 × 15.6
NGC 3077.....	H	800	45	32	2.4 × 24.0
NGC 3077.....	K	800	45	32	2.4 × 24.0
NGC 3077.....	1.64	3000	45	48	2.4 × 24.0
NGC 3077.....	1.70	3000	45	48	2.4 × 24.0
NGC 3077.....	2.09	3000	45	48	2.4 × 24.0
NGC 3077.....	2.14	3000	45	48	2.4 × 24.0
NGC 4214.....	H	800	130	32	2.4 × 12.0
NGC 4214.....	K	800	130	64	2.4 × 12.0
NGC 4449.....	H	800	45	32	2.4 × 9.6
NGC 4449.....	K	800	45	32	2.4 × 9.6
NGC 4449.....	1.63	3000	45	64	2.4 × 9.6
NGC 4449.....	2.14	3000	45	32	2.4 × 9.6
NGC 1569.....	H	800	113	24	2.4 × 4.8
NGC 1569.....	K	800	113	16	2.4 × 4.8
NGC 1569.....	1.64	3000	113	48	2.4 × 4.8
NGC 1569.....	1.70	3000	113	36	2.4 × 4.8
NGC 4861.....	K	800	45	44	2.4 × 12.0
NGC 5253.....	H	800	[a]	100	1.0 × 3.0

[a] Slit in elevation.

trum of the same object given by Lumsden, Puxley, & Doherty (1994) and assuming case B for the Brackett lines while the K spectrum of NGC 4861 was calibrated in the same way using the visible spectrum of McQuade, Calzetti, & Kinney (1995). The latter flux calibrations are not very accurate but in these cases an accurate flux calibration is not required for our analysis.

3. RESULTS AND DISCUSSION

3.1. *Spectra*

The calibrated low-resolution spectra without correction for redshift and reddening are presented in Figure 1. These spectra give an overview of the behavior for each galaxy but are inadequate to estimate fluxes of faint lines, particularly since the continua have stellar absorption features. In critical cases, the galaxies were reobserved at high resolution to confirm and improve the measures of faint emission lines; sample spectra are shown in Figure 2. The observed fluxes and wavelengths for the lines identified in the spectra are given in Table 3. The quoted errors are 1 σ measured at the continuum and do not include the flux calibration uncertainty which is estimated at about 10%. The fluxes are measured by fitting the lines with Gaussians using the task SPLOT in IRAF. In a few cases at low resolution, noise makes the lines appear to exceed the instrumental resolution in width. In these cases the flux is obtained by fitting the line with a Gaussian whose FWHM is set to the instrumental resolution. The presence of many stellar absorption features in the H spectra makes the choice of the continuum level difficult; this additional source of error is considered when we interpret our results in the following sections.

TABLE 2

FLUXES THROUGH SLIT APERTURES

Source	F_H[a]	F_K[a]
He2-10	41.6	19.0
NGC 3077.....	28.1	13.4
NGC 4214.....	3.5	1.4
NGC 4449.....	16.7	8.2
NGC 1569.....	8.3	3.8

[a] 10^{-12} ergs s^{-1} cm^{-2} μm^{-1}.

TABLE 3

DETECTED EMISSION LINES

Object	λ	Flux[a]	Identification
He2-10	1.615	9.1 ± 0.5 (H)	Br13
	1.645	6.0 ± 0.5 (H)	Br12
	1.648	36.5 ± 0.5 (H)	[Fe II]
	1.681	15.5 ± 0.5 (H)	[Fe II]
	1.685	15.2 ± 0.5 (H)	Br11
	1.705	2.2 ± 0.5 (H)	He 4 ^3D–3 ^3P
	1.741	19.0 ± 0.5 (H)	Br10
	2.064	32.5 ± 0.8 (H)	He 2 ^1P–2 ^1S
	2.071	1.0 ± 0.2 (H)	H_2(3, 2)S(5)
	2.078	1.8 ± 0.4 (H)	H_2(2, 1)S(3)
	2.127	5.0 ± 0.1 (H)	H_2(1, 0)S(1)
	2.172	63.0 ± 3	Brγ
NGC 1569.....	1.610	2.9 ± 0.3 (H)	Br13
	1.640	2.9 ± 0.3 (H)	Br12
	1.643	1.7 ± 0.3 (H)	[Fe II]
	1.680	5.7 ± 0.3 (H)	Br11
	1.700	1.2 ± 0.3 (H)	He 4 ^3D–3 ^3P
	1.732	1.1 ± 0.3 (H)(?)	H_2
	1.736	10.1 ± 0.5 (H)	Br10
	2.058	7.0 ± 0.5	He 2 ^1P–2 ^1S
	2.119	1.4 ± 0.5	H_2(1, 0)S(1)
	2.164	19.5 ± 1	Brγ
NGC 3077.....	1.611	11.5 ± 0.5 (H)	Br13
	1.641	4.8 ± 0.2 (H)	Br12
	1.643	11.0 ± 0.5 (H)	[Fe II]
	1.680	12.0 ± 0.5 (H)	Br11
	1.738	16.4 ± 0.5 (H)	Br10
	2.058	13.5 ± 1.5 (H)	He 2 ^1P–2 ^1S
	2.121	2.8 ± 0.5 (H)	H_2(1, 0)S(1)
	2.166	23 ± 3 (H)	Brγ
NGC 4214.....	1.600	4.2 ± 0.7	H_2(6, 4)Q(1)
	1.612	0.9 ± 0.2	H_2(5, 3)O(3)
	1.682	2.5 ± 0.4	Br11
	1.701	1.6 ± 0.3	He 4 ^3D–3 ^3P
	1.738	5.0 ± 1.0	Br10
	2.060	5.4 ± 0.5	He 2 ^1P–2 ^1S
	2.123	1.1 ± 0.4	H_2(1, 0)S(1)
	2.167	9.4 ± 0.7	Brγ
NGC 4449.....	1.644	3.5 ± 1	Br12, [Fe II]
	1.680	2.0 ± 1	Br11
	1.703	2.8 ± 1	He 4 ^3D–3 ^3P
	1.737	2.5 ± 1	Br10
	2.033	0.8 ± 0.2	H_2(1, 0)S(2)
	2.059	3.1 ± 0.4	He 2 ^1P–2 ^1S
	2.067	0.7 ± 0.3	H_2(3, 2)S(5)
	2.120	1.2 ± 0.5	H_2(1, 0)S(1)
	2.153	1.0 ± 0.3	H_2(2, 1)S(2)
	2.166	6.0 ± 0.3	Brγ
NGC 4861.....	2.063	7.3 ± 0.5	He 2 ^1P–2 ^1S
	2.127	1.0 ± 0.5	H_2(1, 0)S(1)
	2.171	20.2 ± 1	Brγ
NGC 5253.....	1.590	3.7 ± 0.3	Br14
	1.613	7.9 ± 0.3	Br13
	1.644	15.0 ± 1.5	Br12, [Fe II]
	1.682	14.8 ± 1	Br11
	1.703	3.2 ± 0.4	He 4 ^3D–3 ^3P
	1.738	16.5 ± 0.5	Br10

[a] 10^{-15} ergs s^{-1} cm^{-2}. Measures at high resolution designated by (H).

The most prominent features detected in the spectra are the emission lines of atomic hydrogen and helium, molecu-

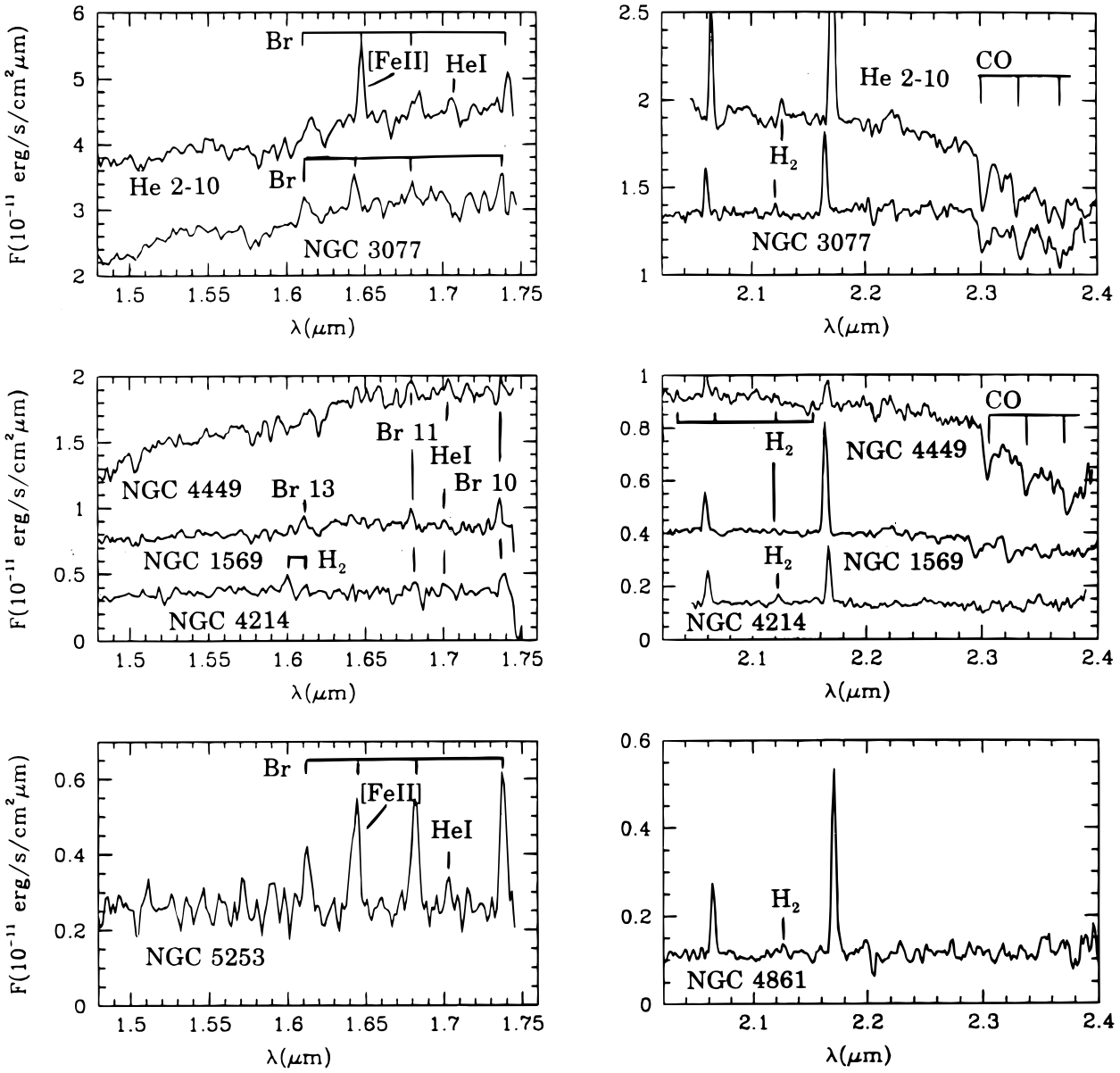

FIG. 1.—Low-resolution infrared spectra of BDGs. Detected emission lines are indicated; for clarity, Brγ (2.166 μm) and He I (2.058 μm) have not been labeled. In addition, the CO absorption bands can be seen in the top four spectra beginning at $\sim$2.3 μm.

lar hydrogen, and forbidden iron, and the absorption features of CO. The ratios of the Brackett lines are consistent within the errors with case B (Hummer & Storey 1987). Small discrepancies from case B in the Br10/Brγ ratio are believed to be due both to extinction and to the uncertainty in the relative calibration of the H and K bands. In the high-resolution spectrum of NGC 3077 the lines Br12 and [Fe II] can be measured separately and Br12 is weaker than expected from case B, probably due to its falling in the CO(7, 4) absorption feature. This same effect also occurs in NGC 1569 and He 2-10.

3.2. *The* K/Brγ *Ratio as Age Indicator*

The K flux emitted by a SB is dominated by the radiation of cool giants and supergiants while the hydrogen recombination lines are due to very young hot stars. Hence, the ratio K/Brγ should be useful as a nearly extinction-independent age indicator for the stellar population.

To test this hypothesis, we measure a spectroscopic CO index applying the procedure defined by Kleinmann & Hall (1986) with one modification. The CO and continuum bands of Kleinmann & Hall are too narrow for our resolution, and the measures would be affected by the noise and the uncertainty in the wavelength calibration. To avoid this problem we define a continuum measure as the level between 2.260 and 2.295 μm and a CO measure as the peak of the CO(0, 2) absorption feature. The spectroscopic index, defined as the difference in magnitudes between the continuum and the CO measure, is transformed into the photometric index following Kleinmann & Hall. In Table 4 the logarithm of K/Brγ and the CO index are presented for our sample of BDGs (K and Brγ for NGC 5253 are from Lumsden et al. 1994). We find a good correlation between the K/Brγ ratio and the presence of the CO stellar absorption features at 2.3 μm.

As another test, we compare with the ratio of the 1.70 μm He I line to Br10 and of [O III]/Hβ. Both of these line ratios are measures of the relative numbers of very hot (>40,000 K) stars, which should be present only in the first stages of a short SB. The correlation of He I/Br10 with K/Brγ is good.

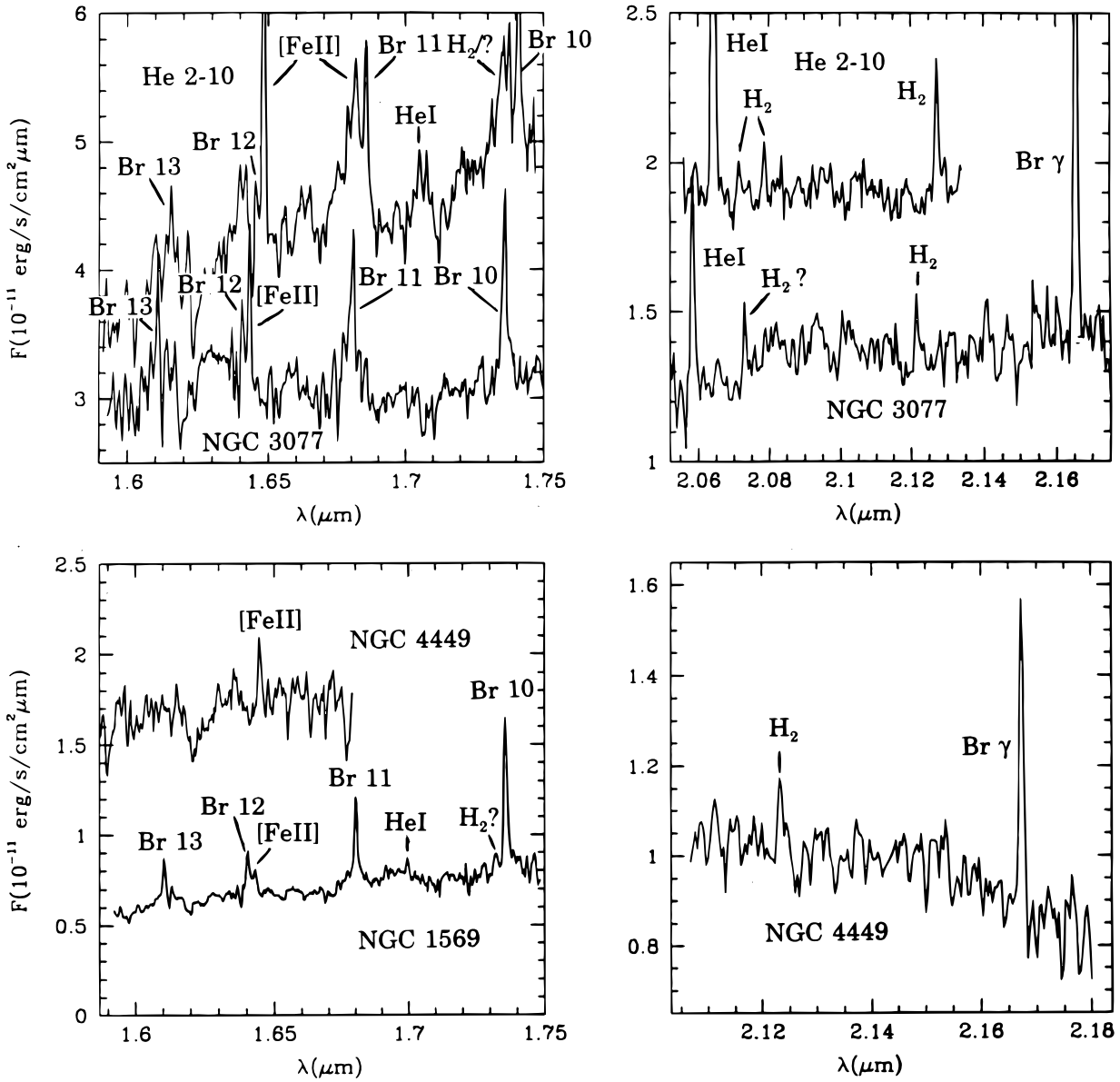

FIG. 2.—High-resolution spectra. Detected emission lines are indicated. The H_2/? blend in He 2-10 near 1.743 μm is also seen in Hubble 12 (Luhman & Rieke 1996).

The ratio [O III]/Hβ behaves roughly as expected, but has a weaker correlation with K/Brγ than the other indicators do.

We calibrate the age dependence of K/Brγ using the starburst model of Rieke et al. (1993). Given an initial mass function (IMF) and a star-formation rate (SFR) the model uses theoretical stellar evolutionary tracks to calculate the values of UV flux, *UBVRJHK* magnitudes, SN rate, and CO index as function of time. We ran the SB model for a Gaussian SFR with FWHM = 5 My and a solar neighborhood IMF (IMF3 in Rieke et al. 1993); K/Brγ as a function of time is calculated from the ratio K/UV given by the model assuming $T = 10^4$ K and case B to convert the UV flux to Brγ strength. The K/Brγ ratio gives us a convenient parameter for comparison with theoretical predictions of [Fe II] emission with age in the following section.

TABLE 4

SPECTRAL PARAMETERS

Object	K/Brγ	CO	He/Br10	[O III]/Hβ
II Zw 40	1.55	0	0.45 ± 0.08	7.3
NGC 4861.....	1.74	0	...	5.2
NGC 5253.....	1.78[a]	...	0.20 ± 0.06	5.2
NGC 4214.....	2.17	0.06 ± 0.01	0.32 ± 0.13	2.6
He2-10	2.48	0.13 ± 0.01	0.12 ± 0.06	1.8
NGC 1569.....	2.64	0.12 ± 0.01	0.12 ± 0.04	5.7
NGC 3077.....	2.80	0.11 ± 0.01	<0.12	2.0
NGC 4449.....	3.28	0.17 ± 0.01	...	3.0

[a] Data from Lumsden et al. 1994.

3.3. *The Excitation of* [Fe II] *Emission*

Strong [Fe II] emission requires large transition zones between H II and H I regions, making thermal excitation in shocks much more efficient than UV fluorescent excitation. The observed ratio [Fe II](1.64)/Brγ in Orion is about 0.06 while galactic and LMC supernova remnants (SNRs) show for the same ratio a typical value of about 30. Therefore, it is often assumed that most of the [Fe II] emission in a SB

arises from SNRs, while most of the Brγ is emitted by H II regions. Forbes & Ward (1994) have attempted to substantiate this assumption on the basis of a correlation between the nonthermal radio fluxes of galaxies at 6 cm with their [Fe II] emission. If one excludes Seyfert galaxies, for which the [Fe II] excitation mechanism may be related to the active galactic nuclei (AGNs), the correlation between radio and [Fe II] fluxes is weak. A strong correlation appears in luminosities, but such relations can easily be a product of selection effects for samples observed to limited sensitivity limits, as is the case for Forbes & Ward's [Fe II] data. The trend of [Fe II] versus 6 cm derived by them falls below the relation for many SNRs (Lumsden & Puxley 1995). Therefore, further confirmation of the expected relation between SNRs and [Fe II] is desirable.

To explore the large scatter in the [Fe II] versus 6 cm plots and the offset between SBs and SNRs, we consider M82 in detail. Lester et al. (1990) measure the [Fe II] emission of M82: summing all their apertures we have a flux of 1.06×10^{-12} ergs s^{-1} cm^{-2}. Because the apertures of Lester et al. cover only the major axis of the galaxy we introduce a correction factor to estimate the total [Fe II] flux. The factor has been calculated on the basis of long-slit spectroscopy of M82 obtained in Brγ with the slit aligned along the minor axis of the galaxy and assuming the same profile luminosity for Brγ and [Fe II]. We take A_V of 5 to 6 as an average value for the effective extinction of the ionized and [Fe II] emitting gas (Satyapal et al. 1995), corresponding to 0.9 mag for the 1.64 μm [Fe II] line. From the various measurements of the distance to M81 (Freedman et al. 1994), we adopt a value of 3.5 Mpc to this galaxy and to M82. We then have an intrinsic [Fe II] flux of 5.7×10^{-12} ergs s^{-1} cm^{-2} and a luminosity $L_{\rm Fe\ II} = 8.4 \times 10^{39}$ ergs s^{-1}.

Following Forbes & Ward (1994), we attempt to relate the [Fe II] luminosity to the radio emission. Adopting the estimate of 3.58 Jy for the 6 cm nonthermal radio flux (Huang et al. 1994), we find roughly 1.5×10^{-12} ergs s^{-1} cm^{-2} of [Fe II] per Jy of radio emission at 6 cm. This value is more than an order of magnitude lower than found for individual SNRs (see, e.g., Lumsden & Puxley 1995). The discrepancy can be understood if the [Fe II]–emitting phase in a supernova remnant lasts less than 10% as long as the energetic electrons producing the nonthermal radio emission. For M82, Rieke et al. (1980) show that the electrons escape into the general interstellar medium where their energy losses are dominated by Compton scattering off far-infrared photons, with resulting lifetimes of $\sim 10^5$ yr. A plausible duration for the [Fe II]-emitting stage is $\sim 10^4$ yr (Lumsden & Puxley 1995). Although these lifetimes are only order-of-magnitude estimates, it is encouraging that they are in the correct ratio to be consistent with the observed values for 6 cm and [Fe II] fluxes. However, we also conclude that the uncorrected comparison between [Fe II] and 6 cm in SNRs and SB galaxies made by Forbes & Ward (1994) is not valid. In fact, this comparison is affected strongly by the conditions controlling the rate of Compton scattering in individual starbursts. In addition to the observed difference between the ratio in supernovae and in M82, the ratio might be expected to vary from one SB to another. Thus, both the offset between [Fe II] and 6 cm between SBs and SNRs and the scatter in this relation for the SBs can be understood qualitatively.

It would be desirable to have a demonstration of the link between the [Fe II] and supernovae in SBs that is more robust than the arguments based on radio emission. Greenhouse et al. (1991) find that two very bright SNRs in M82 have bright [Fe II] emission, suggesting such a link but not yet proving that the bulk of the [Fe II] luminosity of the galaxy is produced in this manner. To make a quantitative comparison, we calibrate the [Fe II](1.64) emission per supernova using M82. The [Fe II] luminosity is given by

$$L_{\rm Fe\ II} = ({\rm SNr}) t_{\rm Fe\ II} L_{\rm Fe\ II/SN}\ , \quad (1)$$

where SNr is the supernova rate, $t_{\rm Fe\ II}$ is the characteristic time for the [Fe II] emission in a SNR, and $L_{\rm Fe\ II/SN}$ is the average luminosity of a SNR in [Fe II]. If the observed SNr in M82 is 0.1 yr^{-1} (Huang et al. 1994), then we obtain

$$L_{\rm Fe\ II/SN} = [L_{\rm Fe\ II}/({\rm SNr}) t_{\rm Fe\ II}] \sim 8 \times 10^{36}\ {\rm ergs\ s^{-1}}\ , \quad (2)$$

where we have assumed $t_{\rm Fe\ II} = 10^4$ yr in the final value (Lumsden & Puxley 1995). This relation is uncertain by at least a factor of 2, since the SNr is uncertain by this amount (Huang et al. 1994). We can compare this value with observations of individual SNRs as summarized by Lumsden & Puxley (1995). They find a typical luminosity in [Fe II] 1.257 μm of $\sim 2 \times 10^{36}$ ergs s^{-1} for bright SNRs in M33 and they cite previous work in the Galaxy and LMC that finds luminosities of $\sim 10^{37}$ ergs s^{-1} for the 1.64 μm line, which is similar in strength to the one at 1.257 μm. They argue that the [Fe II] luminosity is weakly dependent on the density of the interstellar medium (ISM), so these values should transfer roughly to M82. In fact, they are in excellent agreement with our derived average [Fe II] luminosity, demonstrating that the observed rate of supernova explosions would be expected to produce a luminosity in [Fe II] very similar to that observed.

Having demonstrated that supernovae plausibly do account for the [Fe II] emission in M82, we probe whether they generally play this role. We can use the SNr given by the SB model and the calibration from M82 to calculate the values of [Fe II]/Brγ as a function of the age of a burst. We plot a curve in the [Fe II]-Brγ-K diagram (Fig. 3) that represents the expected evolution of ([Fe II] + Br12)/Brγ as a function of K/Brγ. The dots on the curve are separated by 1 My in time and the peak of star formation is located at 5 My (third dot on the curve). Galaxies can most easily deviate from this prediction to the right, particularly if they have relatively weak SBs so the K flux contains a contribution from old stars and the equivalent width of Brγ is reduced from the modeled values. A similar shift might be expected for galaxies with low metallicities and hence reduced iron abundances.

We test the relation by plotting in the [Fe II]-Brγ-K diagram the SB galaxies for which we have the necessary information. Most of the plotted data are from C. Engelbracht (1996) and have been calibrated by assuming the underlying stellar continua have $H-K = 0.2$; the calibration implicitly takes extinction into account. Additional data are taken from Moorwood & Oliva (1988). For their data, the observed [Fe II] + Br12/Brγ ratio has been corrected for the extinction when an extinction value was available. We obtain good agreement between the curve produced by the model and the observational data, particularly if we recall the potential bias for the observations to lie to the right of the predicted curve. This result provides further support of the hypothesis that the [Fe II] in the starbursts arises from supernovae.

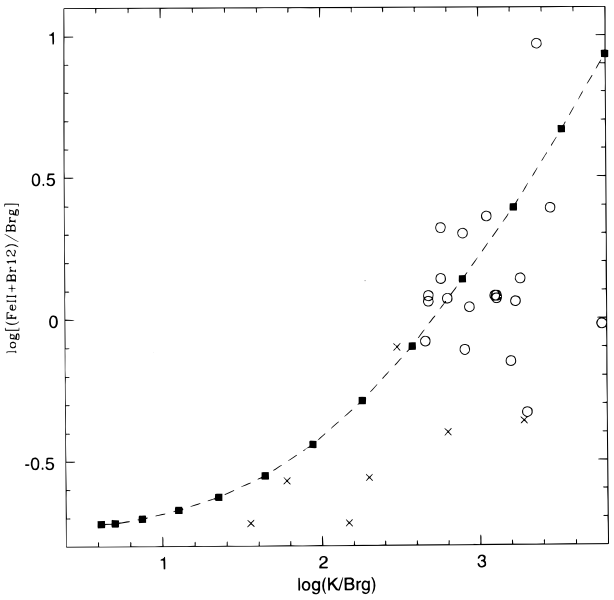

FIG. 3.—Trend of [Fe II] vs. K/Brγ. The dashed line shows the trend predicted by an SB model, assuming a short initial burst of star formation. The boxes are at intervals of 1 million years; the peak of star formation is at the third box from the left at 5 million years. The filled circles show the ratios for luminous SBs, of roughly solar metallicity. The X's are for the BDGs studied in this paper.

We plot the points for our sample of DBGs in the diagram. In our observations, Br12 and [Fe II] are usually unresolved; it is for this reason that we have used the ratio ([Fe II] + Br12)/Brγ ([Fe II]/Brγ can be computed assuming Br12/Brγ = 0.19). Because the extinction is not always known and its value is in many cases controversial we prefer to use the ratio of [Fe II] with the nearest line of the Bracket series reliably detected, usually Br10, and calculate the value of ([Fe II] + Br12)/Brγ assuming case B; this procedure makes our value virtually extinction independent.

From Figure 3, the galaxies NGC 1569, NGC 3077, and NGC 4449 have [Fe II] emission well under the standard SB relation, even though their SBs are old enough to contain evolved stars as indicated by strong CO absorption bands. He 2-10, which also has strong CO, has [Fe II] emission near the standard SB level. This general trend is consistent with the low metallicity of the DBGs, except for the latter galaxy. The dependence of the [Fe II] emission upon the metallicity of the ISM is also in agreement with the supernova-driven origin of this line, which would hypothesize that it is generated as the supernova-driven origin of this line, which would hypothesize that it is generated as the supernova blast wave propagates through the local ISM. II Zw 40, NGC 5253, and NGC 4214 are dominated by extremely young bursts, as indicated by their weak CO absorption, and the [Fe II] emission is very low, as predicted by the model in Figure 3. Therefore, the behavior of the DBGs reinforces the suggestion that the [Fe II] emission in SBs arises primarily from young SNRs.

Given this result, we can use the M82 calibration to derive the following relation:

$$L_{\mathrm{Fe\,II}} \sim (\mathrm{SNr}) \times 8 \times 10^{40}\ \mathrm{ergs\ s^{-1}}\ , \qquad (3)$$

where SNr is in yr^{-1}. Despite the factor of 2 uncertainty due to the remaining uncertainty in the SNr in M82, this relation is potentially a convenient transformation between [Fe II] luminosity and the SNr in SBs.

The K/Brγ ratio constrains the recent star formation of a galaxy. However, the [Fe II]/Brγ ratio depends both on the recent star formation and, through the iron abundance, the star formation integrated over the whole history of a galaxy. Marconi, Matteucci, & Tosi (1994) describe the chemical evolution in BDGs assuming a solar neighborhood IMF and a SFR characterized by several bursts of star formation. Their models indicate a tendency of the O/Fe ratio to decrease and of the Fe/H to increase with the number of past bursts.

To compare with their models, we correct the [Fe II] emission for NGC 1569, NGC 3077, and NGC 4449, using the O/H ratio measured from the visible lines (Storchi-Bergmann, Calzetti, & Kinney 1994; Marconi et al. 1994) and assuming a solar O/Fe ratio. From these assumptions it follows Fe/H $\approx 7 \times 10^{-6}$ (by number) in very good agreement with model 8 of Marconi et al. (1994). On the other hand, the [Fe II] emission from He 2-10 agrees with the SB model with no correction meaning that we can assume a solar Fe/H ratio for this galaxy and using the O/H value given by Vacca & Conti (1992) it follows O/Fe $\approx$ 2.9. Although this value is so low it is out of scale in the plot of Marconi et al., it still follows the general tendency described by model 8. The high level of iron enrichment in this galaxy is an interesting problem for further analysis. For II Zw 40, NGC 5253, and NGC 4214 it is difficult to reach any conclusions because of the extremely low level of [Fe II].

3.4. *Radio—Infrared Relation*

In Figure 4 we plot the logarithm of the radio luminosity at 1.49 GHz versus the logarithm of the far-infrared luminosity for the BDGs in our sample and for the sample of standard starburst galaxies. The far-infrared luminosity has been calculated using the *IRAS* observations and the following equation:

$$\mathrm{FIR(W\ m^{-2})} = 1.26 \times 10^{-14}(2.58F_{60} + F_{100})\ , \qquad (4)$$

where F_{60} and F_{100} are respectively the fluxes at 60 μm and 100 μm measured in Jy (Condon, Anderson, & Helou 1991).

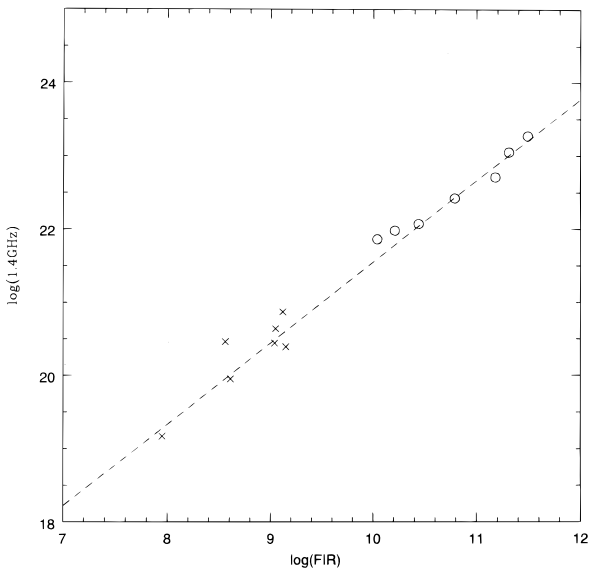

FIG. 4.—Relation between radio and far-infrared fluxes. The open circles are for luminous SBs, of roughly solar metallicity. The X's are for the BDGs studied in this paper.

Although thermal radio emission is often strong in these galaxies, at a frequency as low as 1.49 GHz we can assume the nonthermal component is strong enough that the thermal component does not strongly affect the results in the figure. In Figure 4 we also show the radio/FIR relationship given by Condon et al. for their *IRAS* sample of galaxies. We do not detect any appreciable deviation for the BDGs from the behavior defined by the other galaxies. If we assume the radio emission is due to synchrotron radiation from SNRs and the far-infrared to thermal radiation from dust warmed by hot young stars as suggested by Harwit & Pacini (1975), we infer no anomalous behavior in the number of SNRs or in the dust absorption. We conclude that the low metallicity does not reduce the optical depth of dust in the ultraviolet sufficiently to affect the radio-infrared relation. That is, over the range of metallicity represented by this figure (roughly an order of magnitude), the relations among SNr, [Fe II] emission, nonthermal radio continuum, and far-infrared thermal emission appear to depend on metallicity primarily through the reduction of the iron abundance and hence the relative strength of the [Fe II] lines.

3.5. H_2 *Excitation*

The interpretation of the molecular hydrogen emission is more complex than that of [Fe II]. Both SNRs and H II regions can be quite efficient in the excitation of H_2 leading to H_2/Brγ ratios that are comparable. In proximity to young stars the H_2 can be excited in shocks driven by powerful stellar winds but also directly by fluorescence (Black & van Dishoeck 1987). Further mechanisms such as molecular cloud collisions or large-scale shocks can play an important role, in which case only a fraction of the H_2 emission would be related to the age of the burst. For all these reasons the H_2/Brγ ratio is not expected to be uniquely a function of age. We test this conclusion in the H_2-Brγ-K diagram (Fig. 5), which is similar to the [Fe II]-Brγ-K diagram. For reference, we plot a curve calibrated for H_2 in the same way described in § 3.3 for [Fe II] and assuming all the H_2 from M82 is due to SNRs. As with Figure 3, we expect that the galaxy points would lie to the right of this curve for cases with weak SBs and hence significant portions of their K outputs from old stars. However, the observational points tend to lie above and to the left of the computed trend of H_2/Brγ. It appears that all the galaxies have a minimum level of excitation produced by SNRs, and that this level is not strongly affected by the metallicity of the galaxy. However, most galaxies lie in a region that indicates that other excitation mechanisms play an important role in their H_2 emission.

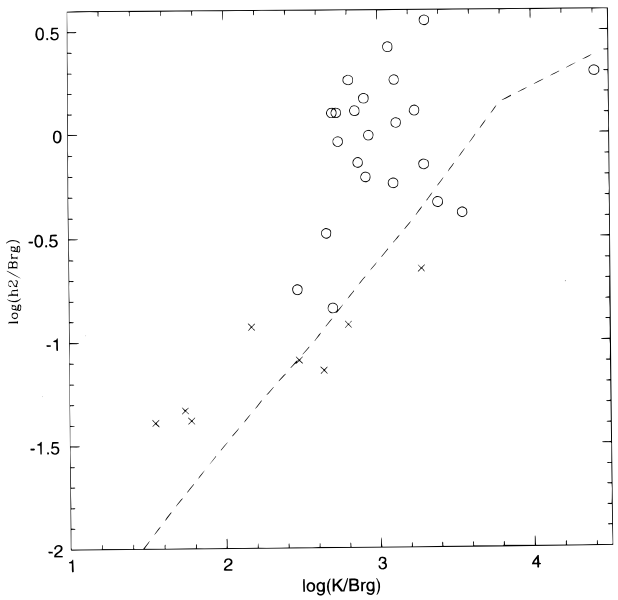

FIG. 5.—Trend of H_2 vs. K/Brγ. The dashed line shows the predictions of the SB model, normalized to M82. The open circles are for luminous SBs, while the X's are for the BDGs studied in this paper.

In fact, we find evidence of fluorescent excitation of molecular hydrogen in He2-10, NGC 4214, and NGC 4449. Beside the transition (1, 0)S(1) at 2.121 μm we detect the transitions (3, 2)S(5) at 2.065 μm and (2, 1)S(3) at 2.072 μm in He 2-10; (3, 2)S(5), (1, 0)S(2) at 2.033 μm and (2, 1)S(2) at 2.154 μm in NGC 4449; while (2, 1)S(3) and (6, 4)Q(1) at 1.600 μm are possibly detected in NGC 4214. All these transitions would be not observable in the case of pure thermal excitation according to the model of Black & van Dishoeck (1987). Similar detections are reported by Vanzi et al. for II Zw 40 and by Lumsden et al. for NGC 5253.

3.6. *Helium Lines*

Vanzi et al. (1996) suggested that the ratio He I(1.7)/Br10 is particularly useful to constrain the temperature of the hot stars in a SB because it is not heavily affected by reddening or electron temperature and the 1.7 μm 4 ^3D–3 ^3P helium line is relatively strong. We detect the 4 ^3D–3 ^3P transition in all our H spectra except those of NGC 3077 and NGC 4449. The measured values for He I(1.7)/Br10 are given in Table 4; the errors are mainly due to the uncertainty in the choice of the continuum. The saturated value for n(He)/n(H) = 0.086 (probably typical for these galaxies) is 0.31 (Vanzi et al. 1996), corresponding to a stellar temperature higher than 40,000 K but below 54,000 K (above this upper temperature limit, helium becomes doubly ionized). All the galaxies but He 2-10, NGC 1569, NGC 3077, and NGC 4449 are consistent with the saturated value.

In Table 4 we also give the values for the ratio [O III](5007)/Hβ taken from the literature. The [O III](5007)/Hβ and [O I](6300)/Hα ratios in He 2-10 were analyzed by Sugai & Taniguchi (1992). They deduce a stellar temperature $T_* = 41{,}000$ K assuming a solar value for the metallicity; temperatures as low as 39,000 K can be justified with lower metallicity. For this galaxy, we can also compare with the mid-infrared fine structure line measurements by Roche et al. (1991). Using Rubin's (1985) nebular models for 0.3 times solar metallicity, we estimate that the data of Roche et al. are compatible with a stellar temperature less than 37,000 K. This limit, as opposed to the more typical 35,000 K, is partly a result of the strong silicate absorption in the galaxy and the consequent low signal-to-noise at 9 μm where the [Ar III] line would lie. The He I/Br10 ratio we obtain indicates a temperature of about 36,000 K. The tendency for [O III]/Hβ to give systematically higher estimates of the stellar temperature than those from He I/Br10 seems to be confirmed by the other three galaxies where the He I is below the saturation value.

Although the 1.7 μm 4 ^3D–3 ^3P helium line and the Br10 line are relatively faint, where they can be measured they should give a very reliable value for the ionizing field temperature. For example, the 1.7 μm He I to Br10 ratio is

virtually independent of electron temperature (Vanzi et al. 1996). Neither hydrogen nor helium is depleted significantly onto grains, and although the ratio is proportional to the helium-to-hydrogen abundance, the variation in this parameter is typically less than a factor of 1.5 in nebular environments. The He I and H recombination lines are produced in virtually the same nebular volume, so their ratio should have little dependence on extinction variations across the source. In addition, the use of infrared lines over a narrow wavelength baseline makes the ratio nearly unaffected by extinction. These virtues have been pointed out previously for use of the 2.06 μm 2 ^1P–1 ^1S He I to Brγ line ratio as a temperature indicator. However, the 2.06 μm line can be amplified by resonance fluorescence, so its strength is strongly influenced by nebular conditions as well as ionizing field temperature (Shields 1993). These complications are absent for the 1.7 μm 4 ^3D–3 ^3P line. In addition, for He2-10 the mid-infrared fine structure lines independently confirm the temperature derived from He I/Br10.

At $\sim$0.4 solar and higher metallicity, it is expected that [O III]/Hβ and other optical indicators will overestimate the temperature of the photoionizing field for a variety of reasons, such as an increase in the electron temperature due to either removal of coolants due to depletion or to heating by photoelectrons released by grains (Shields & Kennicutt 1995). Even though the metallicity in our sample galaxies tends to be at or below this threshold, it appears that temperatures are overestimated in these galaxies by [O III]/Hβ.

4. CONCLUSIONS

The results of this work can be summarized as follows.

1. We have compared the [Fe II](1.64) emission from M82 with the supernova rate. The [Fe II] luminosity of this galaxy agrees well with expectations from supernova remnants observed elsewhere, demonstrating that the [Fe II] emission is predominantly from such objects.

2. Using the calibration derived from M82, we show that [Fe II] emission from galaxies over a range of starburst age and metallicity is consistent with a supernova origin for their [Fe II] also. Including the youngest blue dwarf galaxies, we confirm an overall correlation of [Fe II] with age that is well reproduced by a starburst model assuming that the bulk of the [Fe II] emission rises from supernova remnants.

3. In contrast with the behavior of most of the blue dwarf galaxies, which have [Fe II] emission consistent with low iron abundance, He 2-10 has strong [Fe II] suggesting some peculiarity in its metal-enrichment history or in the [Fe II] excitation.

4. The molecular hydrogen emission in starbursts appears to be excited in a number of ways. There is a minimum emission level that appears to be associated with the supernova rate, but there is also significant scatter above this rate indicating additional excitation mechanisms such as cloud-cloud collisions or fluorescence. In fact, we find evidence for fluorescent excitation in many blue dwarf galaxies.

5. The temperatures of the young stellar populations have been analyzed by means of the helium emission line at 1.7 μm. It appears that there is a tendency for the commonly used [O III]5007/Hβ ratio to overestimate the stellar temperature.

We thank M. Rieke and C. Engelbracht for assistance in obtaining observations. This work was partially supported by NSF; support for L.V. was also provided by the European Community in the framework of the Human and Capital Mobility program.

REFERENCES

Aaronson, M. 1977, Ph.D. thesis, Harvard Univ.
Black, J. H., & van Dishoeck, E. F. 1987, ApJ, 322, 412
Condon, J. J., Anderson, L. M., & Helou, G. 1991, ApJ, 376, 95
Elias, J. H., Frogel, J. A., Matthews, K., & Neugebauer, G. 1982, AJ, 1029
Engelbracht, C. 1996, private communication
Forbes, D. A., & Ward, M. J. 1993, ApJ, 416, 150
Freedman, W. L., et al. 1994, ApJ, 427, 628
Glass, I. S., & Moorwood, A. F. M. 1985, MNRAS, 214, 429
Greenhouse, M. A., Woodward, C. E., Thronson, H. A., Rudy, R. J., Rossano, G. S., Erwin, O., & Peutter, R. C. 1991, ApJ, 383, 164
Harwit, M., & Pacini, F. 1975, ApJ, 200, L127
Huang, Z. P., Thuan, T. X., Chevalier, R. A., Condon, J. J., & Yin, Q. F. 1994, ApJ, 424, 114
Hummer, D. G., & Storey, P. J. 1987, MNRAS, 224, 801
Kleinmann, S. G., & Hall, D. N. B. 1986, ApJS, 62, 501
Lester, D. F., Carr, J. S., Joy, M., & Gaffney, N. 1990, ApJ, 352, 544
Luhman, K. L., & Rieke, G. H. 1996, ApJ, 461, 298
Lumsden, S. L., & Puxley, P. J. 1995, MNRAS, 276, 723
Lumsden, S. L., Puxley, P. J., & Doherty, R. M. 1994, MNRAS, 268, 821
Maiolino, R., Rieke, G. H., & Rieke, M. J. 1996, AJ, 111, 537
Marconi, G., Matteucci, F., & Tosi, M. 1994, MNRAS, 270, 35
McQuade, K., Calzetti, D., & Kinney, A. L. 1995, ApJS, 97, 331
Moorwood, A., & Oliva, E. 1988, A&A, 203, 278
Oliva, E., & Origlia, L. 1992, A&A, 254, 466
Rieke, G. H., Lebofsky, M. J., Thompson, R. I., Low, F. J., & Tokunaga, A. T. 1980, ApJ, 238, 24
Rieke, G. H., Loken, L., Rieke, M. J., & Tamblyn, P. 1993, ApJ, 412, 99
Roche, P. F., Aitken, D. K., Smith, C. H., & Ward, M. J. 1991, MNRAS, 248, 606
Rubin, R. H. 1985, ApJS, 57, 349
Satyapal, S., et al. 1995, ApJ, 448, 611
Shields, J. C. 1993, ApJ, 419, 181
Shields, J. C., & Kennicutt, R. C. 1995, ApJ, 454, 807
Storchi-Bergmann, T., Calzetti, D., & Kinney, A. L. 1994, ApJ, 429, 572
Sugai, H., & Taniguchi, Y. 1992, AJ, 103, 1470
Vacca, W. D., & Conti, P. S. 1992, ApJ, 401, 543
Vanzi, L., Rieke, G. H., Martin, C., & Shields, J. 1996, ApJ, 466, 150
Williams, D. M., Thompson, C. L., Rieke, G. H., & Montgomery, E. F. 1993, Proc. SPIE, 1946, 482